Nanostructures

Mass Production and High Photocatalytic Activity of ZnS Nanoporous Nanoparticles**

Jin-Song Hu, Ling-Ling Ren, Yu-Guo Guo, Han-Pu Liang, An-Min Cao, Li-Jun Wan, and Chun-Li Bai**

Environmental problems associated with organic pollutants and toxic water pollutants provide the impetus for sustained fundamental and applied research in the area of environmental remediation. Semiconductor photocatalysis offers the potential for complete elimination of toxic chemicals through its efficiency and potentially broad applicability.[1] Various new compounds and materials for photocatalysis have been synthesized in the past few decades. A successful example is TiO_2, a metal oxide often used as a catalyst in photochemistry, electrochemistry, environmental protection, and in the battery industry.[2]

Recently, transition-metal sulfides, in particular ZnS and CdS, have been intensively studied because of their unique catalytic functions compared to those of TiO_2.[2,3] These studies have revealed that ZnS nanocrystals (NCs) are good photocatalysts as a result of the rapid generation of electron–hole pairs by photoexcitation and the highly negative reduction potentials of excited electrons. The photocatalytic properties occur not only in the photoreductive production of H_2 from water and the photoreduction of CO_2,[4] but also in the phototransformation of various organic substrates such as the oxidative formation of carbon–carbon bonds from organic electron donors, *cis–trans* photoisomerization of alkenes, and the photoreduction of aldehydes and their derivatives.[5] The notable finding in nonmetalized ZnS photocatalysis is an irreversible two-electron-transfer photoreduction of organic substrates.[6] A favorable shift of the optical response into the visible region occurs subsequent to the doping of transition metal or rare-earth metal ions, such as Ni^{2+} and Cu^{2+}; therefore, ZnS NCs can also be used as effective catalysts for photocatalytic evolution of H_2 and photoreduction of toxic ions under visible-light irradiation.[7]

An important application of ZnS is as a photocatalyst in environmental protection through the removal of organic pollutants and toxic water pollutants. ZnS nanomaterials have been used for the photocatalytic degradation of organic pollutants such as dyes, *p*-nitrophenol, and halogenated benzene derivatives in wastewater treatment.[8] However, the applications of ZnS NCs in photocatalysis are limited to a considerable degree because of the high cost of their large-scale production, coupled with the tremendous difficulties in separation, recovery, and recycling in industrial applications. Nevertheless, the studies have demonstrated that nanoporous materials with high surface-to-volume ratios can be successfully used in various catalysis, environmental engineering, and sensor systems.[9] Some nanoporous materials with regular shapes such as porous nanowires, nanotubes, spheres, and nanoparticles have been successfully prepared by chemical or physical methods,[10] most of which use templates that are intrinsically high in cost and with low production yield. Therefore, the development of cost-effective methods suitable for the large-scale synthesis of ZnS nanoporous nanostructures with high catalytic activity and easy separation represents a critical challenge to their practical applications.

Herein, we report a simple procedure for mass production by using a low-cost, self-assembly synthetic route to produce ZnS nanoporous nanoparticles (NPNPs) composed of building blocks comprising hexagonal wurtzite ZnS nanocrystals of several nanometers in diameter. The advantages of the present protocol are: 1) high surface-to-volume ratios with effective prevention of further aggregation of the nanoparticles, so as to retain high catalytic activities; 2) the profitability of size-quantized, nanometer-sized semiconductor particles with higher redox potentials as a result of the increase in band-gap energy (the energy difference between the lowest unoccupied and highest occupied molecular orbitals),[1,2] which in turn enhances the charge-transfer rates in the system and drastically reduces the volume recombination, that is, radiationless recombination of the electron–hole pair within the semiconductor particle;[11] 3) easier separation and recycling than those obtainable with common NCs because of the larger diameters of NPNPs; and 4) good dispersity and useful dimension without the requirement of constant stirring or a "dark" reaction for adsorption of substrates. In addition, we demonstrate that the ZnS NPNP is an excellent photocatalyst with higher photodegradation efficiency of eosin B in environmental protection than that of TiO_2 nanoparticles.

ZnS NPNPs were prepared by a facile solution-phase thermal decomposition route in the presence of poly(*N*-vinyl-2-pyrrolidone) (PVP). The fine structural details of ZnS NPNPs were investigated by using TEM. Figure 1a shows a low-magnification TEM image of a ZnS sample, which indicates that the sample is composed of a large quantity of well-dispersed spherical nanoparticles with uniform size and shape. The average size of these particles estimated from the TEM image is about 60 nm, which is in good agreement with the result measured by dynamic light scattering (not shown). A typical scanning electron microscope (SEM) image of the sample is presented in Figure 1b, in which the morphology of spherical nanoparticles is also clearly visible. The surface of every particle is rough and with many smaller particles. The high-magnification TEM image in Figure 1c shows many

[*] J.-S. Hu,[+] L.-L. Ren, Y.-G. Guo,[+] H.-P. Liang,[+] A.-M. Cao,[+] Prof. Dr. L.-J. Wan, Prof. Dr. C.-L. Bai
Institute of Chemistry
Chinese Academy of Sciences (CAS)
Beijing 100080 (China)
Fax: (+86) 10-6255-8934
E-mail: wanlijun@iccas.ac.cn
clbai@iccas.ac.cn

[+] Also in the Graduate School of the CAS, Beijing (China)

[**] This work was supported by the National Natural Science Foundation of China (Nos. 20025308 and 20177025), the National Key Project on Basic Research (Grant G2000077501), and the Chinese Academy of Sciences. We thank Dr. L. Jiang for his help in the writing of this manuscript.

Supporting information for this article is available on the WWW under http://www.angewandte.org or from the author.

 DOI: 10.1002/ange.200462057

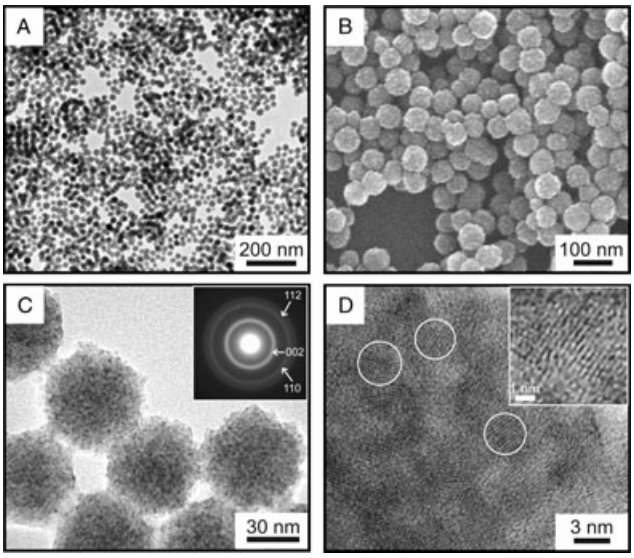

Figure 1. a) Low-magnification TEM image, b) SEM image, c) high-magnification TEM image, and d) HRTEM image of ZnS NPNPs. The inset in (c) is the electron diffraction pattern. The inset in (d) shows the enlarged lattice fringes.

spots with a clear contrast difference in each individual nanoparticle. This observation further confirms that these NPNPs consist of smaller NCs with a size of 3–5 nm which are assembled in a nanoporous structural configuration. A selected-area electron diffraction (ED) pattern of ZnS NPNPs is presented in the inset of Figure 1c. The ED pattern shows a set of concentric rings instead of sharp spots as a result of the small crystallites. The diffraction rings have been indexed to (002), (110), and (112) planes of the hexagonal ZnS phase (JCPDS No. 80-0007). A representative high-resolution TEM (HRTEM) image of ZnS NPNPs in Figure 1d, with an inset image taken on the outside of the particles, shows the lattice fringes of nanocrystals in nanoparticles with a spacing of 0.31 nm, which corresponds to an interplanar distance of the (002) plane of hexagonal ZnS.

The XRD patterns shown in Figure 2 are for ZnS NPNPs obtained at 150 and 180 °C. The diffraction patterns of the two samples are very similar and are in good agreement with hexagonal ZnS (space group: $P6_3/m$ (186)) with lattice constants $a = 3.777$ and $b = 6.188$ Å (JCPDS No. 80-0007). This result illustrates that a heating temperature of 150 °C is sufficient to produce a high-temperature-stable hexagonal ZnS phase in this system. The significant broadening of the diffraction peaks is ascribed to the very small crystallite size within ZnS NPNPs, similar to the case reported in the literature.[12] Moreover, energy-dispersive X-ray (EDX) analysis of ZnS NPNPs (see the Supporting Information) shows two peaks for the elements Zn and S, in addition to the C, O, and Cu derived from the carbon-coated copper TEM grid. These observations show the product is composed of hexagonal ZnS.

Brunauer–Emmett–Teller (BET) gas sorptometry measurements were conducted to examine the porous nature of the ZnS NPNPs. Figure 3 shows the N_2 adsorption/desorption isotherm and the pore-size distribution (inset) of ZnS NPNPs.

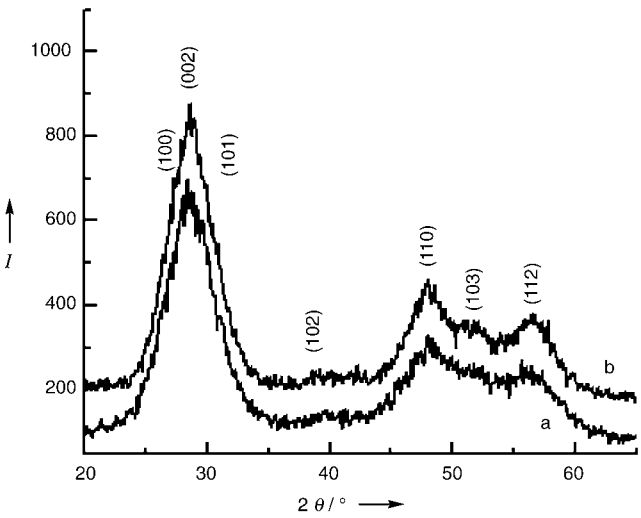

Figure 2. X-ray diffraction pattern of ZnS NPNPs acquired at a) 150 °C and b) 180 °C.

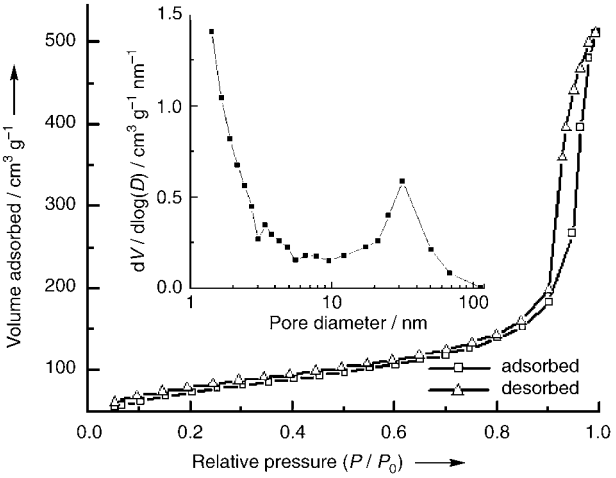

Figure 3. Nitrogen adsorption/desorption isotherm and Barrett–Joyner–Halenda (BJH) pore size distribution plot (inset) of ZnS NPNPs.

The isotherms are identified as type IV, which is characteristic of mesoporous materials. The pore-size distribution obtained from the isotherm indicates a number of pores less than 5 nm in the sample. These pores presumably arise from the spaces among the small nanocrystallites within a ZnS NPNP. The large pores of around 30 nm are attributed to the interparticle spaces. The sharp distribution of the mesopores around 30 nm suggests that the NPNPs have high monodispersity. The BET specific surface area of the sample was calculated from N_2 isotherms at −196.6 °C, and was found to be as much as about 156.1 $m^2 g^{-1}$. The single-point total volume of pores at $P/P_0 = 0.9926$ was 0.59 $cm^{-3} g^{-1}$. The extremely high BET surface area and large total pore volume strongly support the fact that the nanoparticles have a nanoporous structure.

In a series of further experiments we discovered that PVP not only contributed to stabilizing the NPNP assembly but also exerted vigorous control over the formation of the spherical geometry. If no PVP was in the reaction solution,

the small nanoparticles generated initially by the decomposition of complex precursors tended to rapidly aggregate in a random manner, thus leading to the formation of an agglomerate cross-linked by numerous irregular particles (see the Supporting Information). As such, no distinct spherical nanoparticles could be observed. The addition of PVP into the reaction system at a molar ratio of PVP to zinc precursor of 0.04:1 resulted in the sample being mainly composed of spherical particles with plenty of defects that were only partially cross-linked. This finding indicates that the initial nanoparticles tend to assemble into spherical aggregates in the presence of PVP, and any further agglomeration is essentially inhibited by PVP. An increase in the amount of PVP improved the ability to form spherical aggregates and effectively prevented the aggregates from agglomeration. In a typical example in which the molar ratio of PVP to zinc was increased to 0.08, the sample consisted substantially of nanoparticles with regular spherical shape. Therefore, it is clear from the formation process that each spherical particle was produced by aggregation of many smaller nanometer-scale crystallites with a diameter of about 3–5 nm. These spherical nanoparticles were well-separated and had uniform size and shape, such as those shown in Figure 1 a and b.

ZnS has been used as a semiconductor-type photocatalyst for the photoreductive dehalogenation of halogenated benzene derivatives, photocatalytic degradation of water pollutants, and photocatalytic reduction of toxic metal ions.[4–7] To demonstrate the potential applicability of the present ZnS NPNPs in these applications we investigated their photocatalytic activity relative to those of ZnS NCs prepared by a literature method[4c] and of a commercial photocatalyst (Degussa P25 titania), with the photocatalytic degradation of eosin B as a test reaction. The characteristic absorption of eosin B at 517 nm was chosen as the monitored parameter for the photocatalytic degradation process. Figure 4 shows the absorption spectrum of an aqueous solution of eosin B (initial concentration: 5.0×10^{-5} M, 30 mL) in the presence of ZnS NPNPs (10 mg) under exposure to UV light for various durations. The absorption peaks corresponding to the eosin B molecule, such as the sharp peak at 517 nm, diminish gradually as the exposure time increases and completely disappear after about 40 minutes. No new absorption bands appear in either the visible or ultraviolet regions, which indicates the complete photodegradation of eosin B. The color-change sequence in the sample during this process is shown in the inset of Figure 4, from which it is clear that the intense pink color of the starting solution gradually disappears with increasingly longer exposure times.

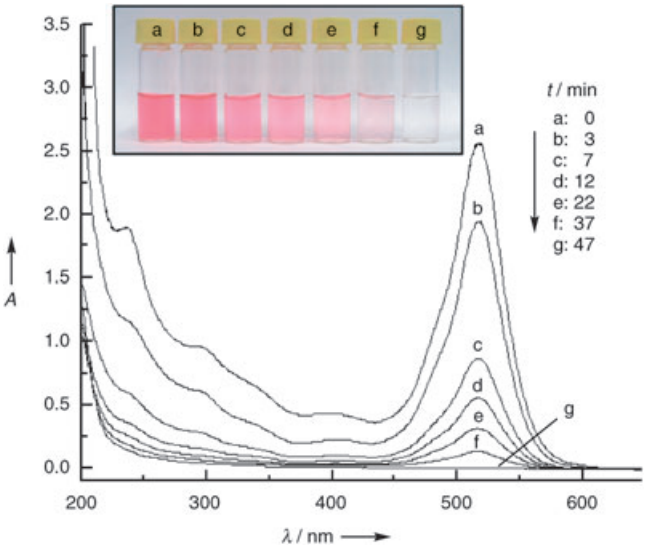

Figure 4. Absorption spectrum of a solution of eosin B (5.0×10^{-5} M, 30 mL) in the presence of ZnS NPNPs (10 mg) under exposure to UV light.

A further comparative experiment was carried out to investigate the catalytic activity. The solution of eosin B was subjected to a series of experimental conditions: a) with Degussa P25 titania (10 mg), in the dark; b) without catalyst, with UV light; c) with ZnS NCs (10 mg), in the dark; d) with ZnS NPNPs (10 mg), in the dark; e) with Degussa P25 titania (10 mg) and UV light; f) with ZnS NCs (10 mg) and UV light; and g) with ZnS NPNPs (10 mg) and UV light. The results are illustrated in Figure 5. Under the experimental conditions

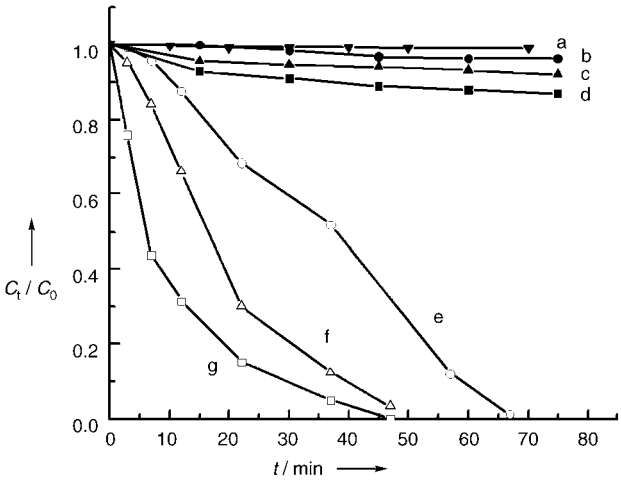

Figure 5. Photodegradation of eosin B (5.0×10^{-5} M, 30 mL) under different conditions: a) with Degussa P25 titania (10 mg), in the dark; b) without any catalyst, with UV light; c) with ZnS NCs (10 mg), in the dark; d) with ZnS NPNPs (10 mg), in the dark; e) with Degussa P25 titania (10 mg) and UV light; f) with ZnS NCs (10 mg) and UV light; g) with ZnS NPNPs (10 mg) and UV light.

from (a) to (d), the photocatalytic effect on the solution degradation without catalysts but under exposure to UV light is almost the same as that with catalyst but no exposure to UV light. For example, a slight decrease in the concentration of eosin B was detected in the absence of any catalyst (curve b). Exposure to UV light for 1.5 h resulted in only 5% degradation of this compound. A slight decrease in the concentration of eosin B took place in the presence of ZnS NPNPs (curve d) and ZnS NCs (curve c) in the dark, compared to that in the presence of Degussa P25 (curve a) in the dark. This decrease may be mainly ascribed to the adsorption of eosin B on the porous nanostructures, although without exposure to UV light. The concentration of he

eosin B solution hardly changed after mixing the solution with catalysts for 15 minutes, which indicates that the adsorption of eosin B on nanostructured catalysts reached an equilibrium state. However, from the data in curves e (Degussa P25), f (ZnS NCs), and g (ZnS NPNPs), it is clearly seen that, under identical conditions with exposure to UV light, the ZnS NPNP photocatalyst shows much greater activity than that of Degussa P25 or ZnS NCs. The degradation of eosin B in the ZnS NPNPs follows first-order kinetics. Exposure of the solution of eosin B to UV light for about 40 minutes resulted in complete decolorization. This difference in the photocatalytic activity between ZnS NPNPs and Degussa P25 can be explained by the larger specific surface area of the former (ca. 156.1 m^2g^{-1} versus Degussa P25 powder ca. 45 m^2g^{-1}), and hence the stronger adsorption of the ZnS NPNPs to the molecules of eosin B. The photocatalytic superiority of ZnS NPNPs over ZnS NCs may be influenced by the unwanted aggregation of ZnS NCs during the reaction, which leads to a rapid decrease in the active surface area, while ZnS NPNPs maintain an excellent porous nanostructure and are effectively prevented from aggregating. A more detailed understanding of the photocatalytic activity of ZnS NPNPs is currently under way.

In conclusion, we have developed a simple and robust method to produce ZnS nanoporous nanoparticles on a large scale. These NPNPs are uniform spheres, monodispersed in size at around 60 nm in diameter, and are formed by a self-assembly process of hexagonal ZnS nanocrystals of 3–5-nm size as building blocks. They possess a specific surface area on the order of 156 m^2g^{-1}, which leads to substantially more effective photocatalytic performance compared to that of Degussa P25 titania or ZnS NCs, as demonstrated in the photodegradation of eosin B at ambient temperature. A combination of their unique features of high surface-to-volume ratios, monodispersion, and rich photocatalytic and luminescent properties suggests that these ZnS NPNPs will find many interesting applications in semiconductor photocatalysis, inorganic light-emitting diodes (ILEDs), solar cells, environmental remediation, and nanodevices.

Experimental Section

Preparation of ZnS NPNPs: Zinc acetate, thiourea, and ethylene glycol were obtained from Beijing Chemical Reagent Ltd., China, in the highest purity and used directly without further purification. Poly(*N*-vinyl-2-pyrrolidone) (PVP, $M_w = 58000$) was obtained from Sigma-Aldrich Chemical Co., USA. Ultrapure water with a resistivity of 18.2 MΩ cm, produced by using a Milli-Q apparatus (Millipore), was used in all the experiments. ZnS NPNPs were produced by a precursor thermolysis route in the presence of ethylene glycol as the reaction medium. In a typical experiment, zinc acetate (6 mmol) and thiourea (12 mmol) were dissolved in ethylene glycol (150 mL). PVP (4.8 g) was then added to the solution with stirring and, after its complete dissolution, the clear solution was heated to 150 °C. After about 10 min the solution turned milky white, which indicated the initial formation of ZnS nanocrystals. The mixture was maintained at 150 ± 5 °C for 3 h and the color of the reaction solution became milky white mixed with light yellow. The ZnS NPNPs obtained were separated from the reaction mixture by centrifugation, and washed several times with ultrapure water and ethanol to remove the impurities and PVP. Finally, the ZnS NPNPs were dried in a vaccum oven (ca. 0.1 MPa) for 6 h prior to being characterized.

Preparation of ZnS NCs: ZnS nanocrystallites were prepared by using the method described in the literature.[4c] Briefly, the ZnS NC samples were prepared in an argon atmosphere by mixing equal amounts of aqueous 0.05 M solutions of $ZnSO_4$ and Na_2S in an ice bath with stirring. TEM images showed that the so-prepared ZnS NCs had a diameter ranging from 3 to 5 nm, and easily aggregated.

Characterization: For TEM observation, the samples were redispersed in water or ethanol by ultrasonic treatment and dropped on carbon–copper grids. TEM images were collected by using a JEOL JEM 2010F microscope working at 200 kV and equipped with an energy-dispersive X-ray analyzer (Phoenix). A Hitachi S-4300F scanning electron microscope (SEM) was used to investigate the morphology of the hollow spheres.

X-ray powder diffraction (XRD) measurements were carried out with a Rigaku D/max-2500 instrument using filtered $Cu_{K\alpha}$ radiation. The nitrogen adsorption and desorption isotherms at 77 K were measured using a Micrometrics ASAP 2010 system after the sample was degassed in vacuum at 130 °C overnight. A Shimadzu UV-1601PC spectrophotometer was used to record the UV/Vis spectra of various samples.

Photocatalytic activity measurement: A cylindrical pyrex flask (capacity ca. 40 mL) was used as the photoreactor vessel. The reaction system containing eosin B ($C_{20}H_6Br_2N_2Na_2O_9$, Sigma-Aldrich Chemical Co.; 5.0×10^{-5} M, 30 mL) and ZnS NPNP catalyst (10 mg) was magnetically stirred in the dark for 15 min to reach the adsorption equilibrium of eosin B with the catalyst, and then exposed to light from a Philips HPK high-pressure Hg lamp (125 W). Commercial TiO_2 (Degussa P25, Degussa Co.) was adopted as the reference with which to compare the photocatalytic activity under the same experimental conditions. UV/Vis absorption spectra were recorded at different intervals to monitor the reaction.

Received: September 21, 2004
Published online: January 14, 2005

Keywords: nanostructures · photocatalysis · self-assembly · semiconductors · zinc

[1] a) M. R. Hoffmann, S. T. Martin, W. Choi, D. W. Bahnemann, *Chem. Rev.* **1995**, *95*, 69–96; b) M. Anpo, M. Takeuchi, *J. Catal.* **2003**, *216*, 505–516.

[2] a) I. Salem, *Catal. Rev. Sci. Eng.* **2003**, *45*, 205–296; b) A. L. Linsebigler, G. Lu, J. T. Yates, Jr., *Chem. Rev.* **1995**, *95*, 735–758.

[3] a) S. Yanagida, K. Mizumoto, C. J. Pac, *J. Am. Chem. Soc.* **1986**, *108*, 647–654; b) S. Yanagida, T. Azuma, Y. Midori, C. J. Pac, H. Sakurai, *J. Chem. Soc. Perkin Trans. 2* **1985**, 1487–1493; c) W. F. Shangguan, A. Yoshida, *J. Phys. Chem. B* **2002**, *106*, 12227–12230; d) G. Q. Guan, T. Kida, K. Kusakabe, K. Kimura, X. M. Fang, T. L. Ma, E. Abe, A. Yoshida, *Chem. Phys. Lett.* **2004**, *385*, 319–322.

[4] a) H. Fujiwara, H. Hosokawa, K. Murakoshi, Y. Wada, S. Yanagida, *Langmuir* **1998**, *14*, 5154–5159; b) A. Koca, M. Sahin, *Int. J. Hydrogen Energy* **2002**, *27*, 363–367.

[5] a) S. Yanagida, H. Kawakami, Y. Midori, H. Kizumoto, C. J. Pac, Y. Wada, *Bull. Chem. Soc. Jpn.* **1995**, *68*, 1811–1823; b) M. Kanemoto, T. Shiragami, C. J. Pac, S. Yanagida, *J. Phys. Chem.* **1992**, *96*, 3521–3526; c) T. Shiragami, H. Ankyu, S. Fukami, C. J. Pac, S. Yanagida, H. Mori, H. Fujita, *J. Chem. Soc. Faraday Trans.* **1992**, *88*, 1055–1061; d) S. Marinković, N. Hoffmann, *Eur. J. Org. Chem.* **2004**, 3102–3107; e) G. Hörner, P. Johne, R. Kunneth, G. Twardzik, H. Roth, T. Clark, H. Kisch, *Chem. Eur. J.* **1999**, *5*, 208–217.

[6] a) S. Yanagida, Y. Ishimaru, Y. Miyake, T. Shiragami, C. J. Pac, K. Hashimoto, T. Sakata, *J. Phys. Chem.* **1989**, *93*, 2576–2582;

b) S. Yanagida, H. Kizumoto, Y. Ishimaru, C. J. Pac, H. Sakurai, *Chem. Lett.* **1985**, 141.
[7] a) I. Tsuji, A. Kudo, *J. Photochem. Photobiol. A* **2003**, *156*, 249 – 252; b) A. Kudo, M. Sekizawa, *Catal. Lett.* **1999**, *58*, 241 – 243; c) A. Kudo, M. Sekizawa, *Chem. Commun.* **2000**, 1371 – 1372; d) O. Hamanoi, A. Kudo, *Chem. Lett.* **2002**, 838 – 839.
[8] a) J. Dai, Z. Jiang, W. Li, G. Bian, Q. Zhu, *Mater. Lett.* **2002**, *55*, 383 – 387; b) H. Yin, Y. Wada, T. Kitamura, S. Yanagida, *Environ. Sci. Technol.* **2001**, *35*, 227 – 231; c) C. L. Torres-Martínez, R. Kho, O. I. Mian, R. K. Mehra, *J. Colloid Interface Sci.* **2001**, *240*, 525 – 531; d) Y. Wada, H. Yin, T. Kitamura, S. Yanagida, *Chem. Commun.* **1998**, 2683 – 2684; e) X. Wang, S. O. Pehkonen, A. K. Ray, *Ind. Eng. Chem. Res.* **2004**, *43*, 1665 – 1672.
[9] a) J. C. Yu, L. Zhang, Z. Zheng, J. Zhao, *Chem. Mater.* **2003**, *15*, 2280 – 2286; b) D. M. Antonelli, J. Y. Ying, *Angew. Chem.* **1995**, *107*, 2202 – 2206; *Angew. Chem. Int. Ed. Engl.* **1995**, *34*, 2014 – 2017; c) Y. Ding, M. Chen, J. Erlebacher, *J. Am. Chem. Soc.* **2004**, *126*, 6876 – 6877; d) Y. L. Wang, X. C. Jiang, Y. N. Xia, *J. Am. Chem. Soc.* **2003**, *125*, 16176 – 16177.
[10] a) X. D. Wang, C. J. Summers, Z. L. Wang, *Adv. Mater.* **2004**, *16*, 1215 – 1218; b) C. X. Ji, P. C. Searson, *J. Phys. Chem. B* **2003**, *107*, 4494 – 4499; c) F. Li, J. He, W. L. Zhou, J. B. Wiley, *J. Am. Chem. Soc.* **2003**, *125*, 16166 – 16167; d) D. G. Shchukin, R. A. Caruso, *Chem. Mater.* **2004**, *16*, 2287 – 2292; e) J. Jiang, A. Kucernak, *Chem. Mater.* **2004**, *16*, 1362 – 1367; f) K. Suzuki, K. Ikari, H. Imai, *J. Am. Chem. Soc.* **2004**, *126*, 462 – 463.
[11] Z. Zhang, C. C. Wang, R. Zakaria, J. Y. Ying, *J. Phys. Chem. B* **1998**, *102*, 10871 – 10878.
[12] a) Y. Zhao, Y. Zhang, H. Zhu, G. C. Hadjipanayis, J. Q. Xiao, *J. Am. Chem. Soc.* **2004**, *126*, 6874 – 6875; b) J. Nanda, S. Sapra, D. D. Sarma, N. Chandrasekharan, G. Hodes, *Chem. Mater.* **2000**, *12*, 1018 – 1024.

